CRYSTAL GROWTH & DESIGN
2008
VOL. 8, NO. 7
2144–2149

Synthesis, Characterization, and Electrical Properties of SiCN Nanowires

Kefeng Cai,*,† Linyong Huang,‡ Aixia Zhang,† Junlin Yin,§ and Hong Liu‡

Tongji University, Functional Materials Research Laboratory, 1239 Siping Road, Shanghai 200092, China, State Key Laboratory of Crystal Materials, Bio-micro/nano Functional Materials Center, Shandong University, 27 Shanda South Road, Jinan 250100, China, and Tongji University, Shanghai Key Laboratory of Development and Application for Metal-Functional Materials, 1239 Siping Road, Shanghai 200092, China

Received October 31, 2007; Revised Manuscript Received April 29, 2008

ABSTRACT: SiCN nanowires are prepared by pyrolysis of hexamethyldisilazane using ferrocene as a catalyst precursor with or without thiophene, at 1100 °C in a flowing Ar atmosphere. The SiCN nanowires are about 10−60 nm in diameter and on the millimeter scale in length. The addition of thiophene is found to be effective in promoting the growth of SiCN nanowires. A vapor−liquid−solid growth mechanism of the nanowires is proposed. Electrical resistivity of a single SiCN nanowire is measured at room temperature for the first time.

Introduction

Silicon carbonitride (SiCN) has potential applications in high temperature semiconducting devices[1] and is an excellent candidate for a reinforcing phase in ceramic-, metal-, and polymer-matrix composites[2] due to its excellent physical and chemical properties, such as high thermal conductivity, high hardness, excellent thermal stability, wide band gap characteristics, high mechanical strength, high temperature oxidation resistance, and chemical inertness.[3,4] Theoretical calculations indicate that the chemical and physical properties of one-dimensional (1D) nanostructures are superior to those of bulk or thin film.[5] Therefore, it is advantageous to prepare SiCN 1D nanostructures. In 2000, Tantair et al.[6] prepared SiCN nanorods of 20−25 nm in diameter and 1−1.5 μm in length by using a two-stage growth method and reported their field emission properties for the first time. Field emission characteristics of the SiCN nanorods showed a low turn-on field with relatively high current density. The stability of field emission from such nanorods is better than that of carbon nanotubes or carbon-coated-Si microtips.[6] Since then much attention has been paid to the synthesis and properties of 1D SiCN nanostructures. Luo et al.[7] synthesized SiCN polycrystalline nanorods of 20−200 nm in diameter and 2 μm in length from the mixture of polytitanosilazane and silicon powders at 1350 °C in N_2. Cheng et al.[8] synthesized SiCN cones with nanometer-sized tips on Si wafers using an ellipsoid microwave plasma chemical vapor deposition (CVD) reactor with gas mixture of CH_4, SiH_4, Ar, H_2, and N_2 as precursors. The SiCN cones showed very good field emission properties with a low turn on field of 0.6 V/μm and the field emission current density of 4.7 mA/cm^2 at an applied field of 2.8 V/μm. Chang et al.[9] synthesized SiCN nanotubes by a microwave plasma CVD method using CH_4 and H_2 or N_2 as gas sources, Si columns as additional Si solid sources, and Fe, Fe−Y and Co−Ni as catalysts. They also studied the field emission properties of the SiCN nanotubes and found that the emission current density was over 10 mA/cm^2 at 10 V/μm.

Organic precursors are the best candidates for synthesis of 1D nanostructures. There is a great deal of literature related to the synthesis of carbon nanotubes from pyrolysis of hydrocarbon compounds, such as methane, acetylene, benzene, and so on.[10–22] This methodology has also been used for synthesis of 1D SiC nanostructures. For example, Yang et al.[23] obtained SiC nanorods of 80−200 nm in diameter and ∼4 μm in length by pyrolysis of polyureasilazane using $FeCl_2$ as a catalyst precursor at 1700 °C for 2 h in a flowing N_2. Zhang et al.[24] reported the synthesis of SiC nanorods by a floating catalyst method using $SiCl_4$−C_6H_6 as the source of silicon and carbon, ferrocene as a catalyst precursor, and thiophene as an additive in a mixture of Ar and H_2 at 1100−1200 °C. However, the system they used was complicated, and the product was not uniform. Hexamethyldisilane (HMDS, Me_6Si_2, Me═CH_3) and hexamethyldisilazane (HMDSN, $(Me_3Si)_2NH$) have been extensively employed as precursors for synthesizing SiC and SiCN ceramics.[25–30] Recently, we[31] developed a method to prepare ultralong (1−2 mm long) SiC and SiCN nanowires by pyrolysis of HMDS and HMDSN, respectively, in a flowing Ar atmosphere at 1200 °C. However, the yield was still low and the diameter of the nanowires is in the range of about 15−110 nm. Ferrocene and thiophene have been demonstrated to be an efficient catalyst precursor[14,16,22,32,33] and promoter,[16] respectively, for the synthesis of carbon nanotubes. Both of the above chemicals could have the same function for synthesis of SiCN nanowires. In addition, it is well-known that using ferrocene and thiophene will result in 1D nanostructures each with a nanoparticle at their tips; however, the exact composition and phase structure of the nanoparticles have rarely been studied. In this work, a pyrolysis of HMDSN catalyzed by ferrocene with or without thiophene was investigated. SiCN nanowires of 10−60 nm in diameter and on the millimeter scale in length were obtained. The microstructure, growth mechanism, and electrical properties of the nanowires as well as the composition and phase structure of the nanoparticles at the tips of the nanowires were studied.

Experimental Procedures

The synthesis was carried out in a system described in our previous work (see schematic diagram of the system in ref 31). Briefly, the system contained a quartz tube (inner diameter ∼85 mm) with one end sealed. The sealed end was put in the hot zone of an electric muffle

* To whom correspondence should be addressed. Tel./Fax: +86-21-65980255; e-mail: kfcai@mail.tongji.edu.cn; web: http://www.tongji.edu.cn/∼fmrl.
† Functional Materials Research Laboratory, Tongji University.
‡ Shandong University.
§ Shanghai Key Laboratory of Development and Application for Metal-Functional Materials, Tongji University.

10.1021/cg701079x CCC: $40.75
Published on Web 06/17/2008

furnace. In a typical synthesis, about 8 mL of analytical pure HMDSN and 0.1 g of ferrocene were placed in a 10-mL corundum crucible and the crucible was put on a mullite firebrick (~150 × 80 × 12 mm^3). As thiophene was also used, a 5-mL corundum crucible loaded with ~2 mL of thiophene (99% purity, Alfa Aeser) was placed on the mullite firebrick beside the 10-mL crucible at the downstream side. The firebrick was carefully pushed into the hot zone of the quartz tube. After eliminating the air in the tube furnace, the furnace was heated up to ~1100 °C at a rate of 10 °C/min, and held at 1100 °C for 3 h, in a flowing Ar at a flowing rate of ~8 mL/min. The furnace was cooled from the synthesis temperature down to 700 °C in 10 h, and then cooled naturally to room temperature. White wool-like product (~2 mm thick, see Supporting Information) was observed on the surface of the firebrick. The thickness of the product was similar to that of the nanowires from pyrolysis of pure HMDSN.

The morphology, crystal structure, and composition of the product were examined by powder X-ray diffraction (XRD, Rigaku, D/max2550), scanning electron microscopy (SEM, JSM5510), transmission electron microscopy (TEM, H-800), and high-resolution TEM (HRTEM, JEM-2100F, JEOL) equipped with energy dispersive X-ray spectroscopy (EDS), respectively.

For SEM samples, a small amount of product was stripped from the firebrick and stuck on the surface of a carbon film. The carbon film itself was bonded on an aluminum pellet. For the TEM sample, the product was gently ground with an agate mortar for a few seconds and then ultrasonically dispersed in ethanol for 1 h before being dropped on a copper grid coated with carbon film.

In order to characterize the electrical transport properties, a device was prepared as follows: (1) Droplets of the well-dispersed suspension were applied onto a quartz glass slide. (2) A separated nanowire was located on the slide via microscopy. (3) A pair of electrodes was prepared by connecting two thin copper wires on the tops of the nanowire with two small droplets of conducting silver resin (purchased from SPI) under the microscope. The I−V measurement was carried out on a Keithley 4200 system at room temperature.

Results and Discussion

A thin wool-like layer (abbreviated as Product a in the following text) can be obtained by pyrolyzing HMDSN at 1100 °C when ferrocene is added in the precursor. When both ferrocene and thiophene are used, a thick layer of wool-like product (abbreviated as Product b in the following text) is obtained. Our previous work shows that no wool-like product is found by pyrolyzing pure HMDSN at 1100 °C.[31] This indicates that adding ferrocene can reduce the synthesis temperature and that thiophene can promote the growth of the product.

SEM observation indicates that both the products have the same morphology. An SEM image and XRD pattern of the products are shown in Figure 1. Figure 1a shows a typical SEM image of the products. It reveals that the products mainly consist of nanowires. The length of the nanowires is too long to be measured under SEM. They are estimated to be on the millimeter scale from the observation under the optical microscope. Figure 1b shows the XRD patterns of the Products a and b. Three peaks at ~35.6°, 59.9°, and 71.7° are observed in both the XRD patterns. These three peaks can be indexed to the (111), (220), and (311) plane peaks of SiCN (JCPDS card file, no.74-2309), respectively, indicating the formation of SiCN. A small wide peak at ~34° is probably related to carbon from pyrolysis of HMDSN and stacking faults.[34] Additional peaks at 28.3° and 47.4° in the pattern of Product b correspond to FeS (JCPDS card file, no. 23-1123). And the peak at ~29.9° in the pattern of Product b correspond to Fe_3S_4 (JCPDS card file, no. 89-1998). Chen et al.[16] also found FeS and Fe_3S_4 in the product when they synthesized carbon nanotubes by pyrolysis of benzene catalyzed by ferrocene and thiophene, but they did not give details.

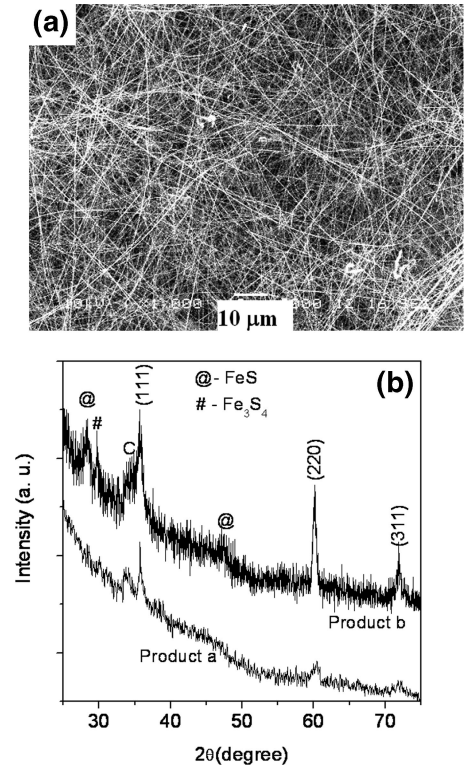

Figure 1. (a) A typical SEM image of the products and (b) XRD patterns of the products.

Figure 2a−d are TEM and HRTEM images of the SiCN nanowires. Figure 2a shows a typical low-magnification TEM image of Product a. Most nanowires are uniform except several nanowires with "Y" junctions. The diameters of most nanowires are in the range of about 10−60 nm. Figure 2b is TEM image at high magnification of the zone indicated by a black square in Figure 2a. The nanowire labeled by a white arrow has "Y" junction. And there is a twin in the middle of the nanowire marked by two black arrows. Thick nanowires possess a high density of stacking faults, which are perpendicular to the wire axes. Spherical nanoparticles are observed at the tips of the nanowires (see the spherical nanoparticle indicated by a black arrow in Figure 2b. EDS analysis indicates that such nanoparticles contain Fe and SAED analysis (see SAED pattern in Figure 2c reveals that the spherical nanoparticles are cubic Fe. Although both Products a and b are composed of nanowires with similar length and diameter, more nanowires with "Y" junction can be found in Product b, which is probably due to the effect of sulfur from thiophene.[35] The significant difference between Products a and b is that the nanoparticles at the tips of nanowires in Product b are faceted rather than spherical (see the nanoparticle indicated by an arrow in Figure 2d). EDS analysis indicates that such nanoparticles contain Fe and S. HRTEM images (Figure 2e) indicate that the faceted nanoparticle is single crystalline. The spacing between two adjacent lattice planes is about 0.20 nm that is close to the spacing of (220) planes of FeS (JCPDS card file, No. 23-1123), which indicates that the nanoparticles are FeS. SAED analysis (see SAED pattern in Figure 2f) confirms that such faceted nanoparticles are cubic FeS.

EDS spectrum, TEM image, and HRTEM images taken from the rod parts of the nanowires are shown in Figure 3. The morphology of the rod parts of the nanowires from Product a is quite similar to that of Product b. All the nanowires can be divided into two categories. One has perfect lattice planes, and

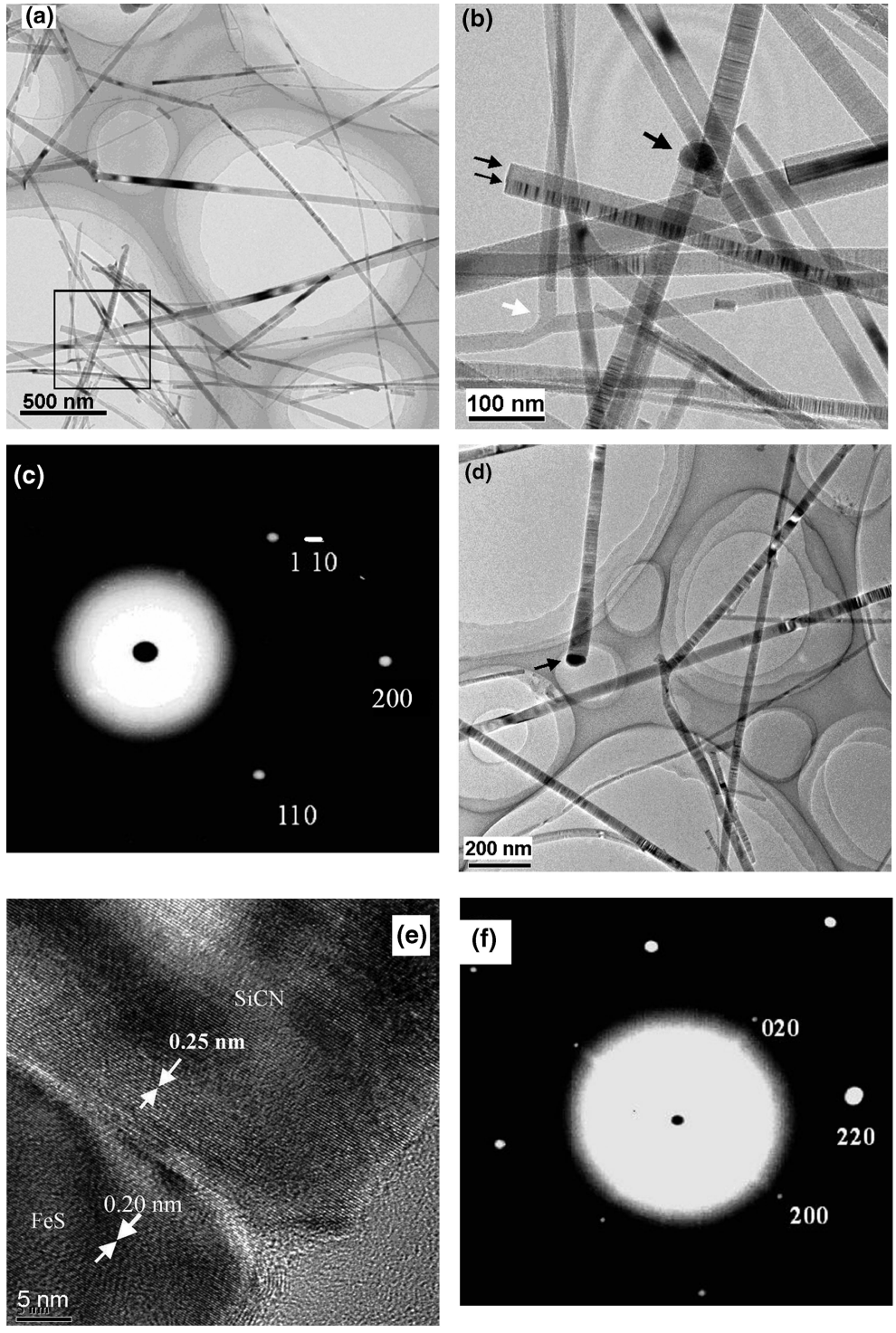

Figure 2. (a) A typical TEM image of the SiCN nanowires at low magnification of Product a, (b) TEM image at high magnification of the zone indicated by the square in (a), (c) SAED pattern taken on a spherical nanoparticle, (d) TEM image of the SiCN nanowires of Product b at low magnification, (e) HRTEM image of a joint between the rod part and the faceted nanoparticle in (d), and (f) SAED pattern taken on a faceted nanoparticle.

the distance between two adjacent lattice planes is about 0.25 nm, which is close to the spacing of (111) planes of cubic SiCN (JCPDS card file, No. 74-2309) (see Figure 3a). Another has many microtwins and stacking faults (see Figure 3b). The inset in Figure 3b is the SAED pattern taken on the nanowire also showing the stacking fault characteristic. The rod parts of the nanowires from these two products have almost the same composition according to EDS analysis. Figure 3c shows a typical EDS spectrum collected from the rod parts of the nanowires. It shows the presence of silicon, carbon, and nitrogen. The peaks of copper must be originated from the copper grid of the TEM sample holder. The peak of oxygen should come from a thin amorphous SiO_2 layer on the surface of the nanowires (see Figure 3a). Occasionally, twin planes in some twin-structured nanowires are along the central line of the nanowires (see Figures 2b and 3d). One half of the nanowire has perfect lattice planes, and the other is full of stacking faults (Figure 3e). The nanowires with the "Y" junction usually

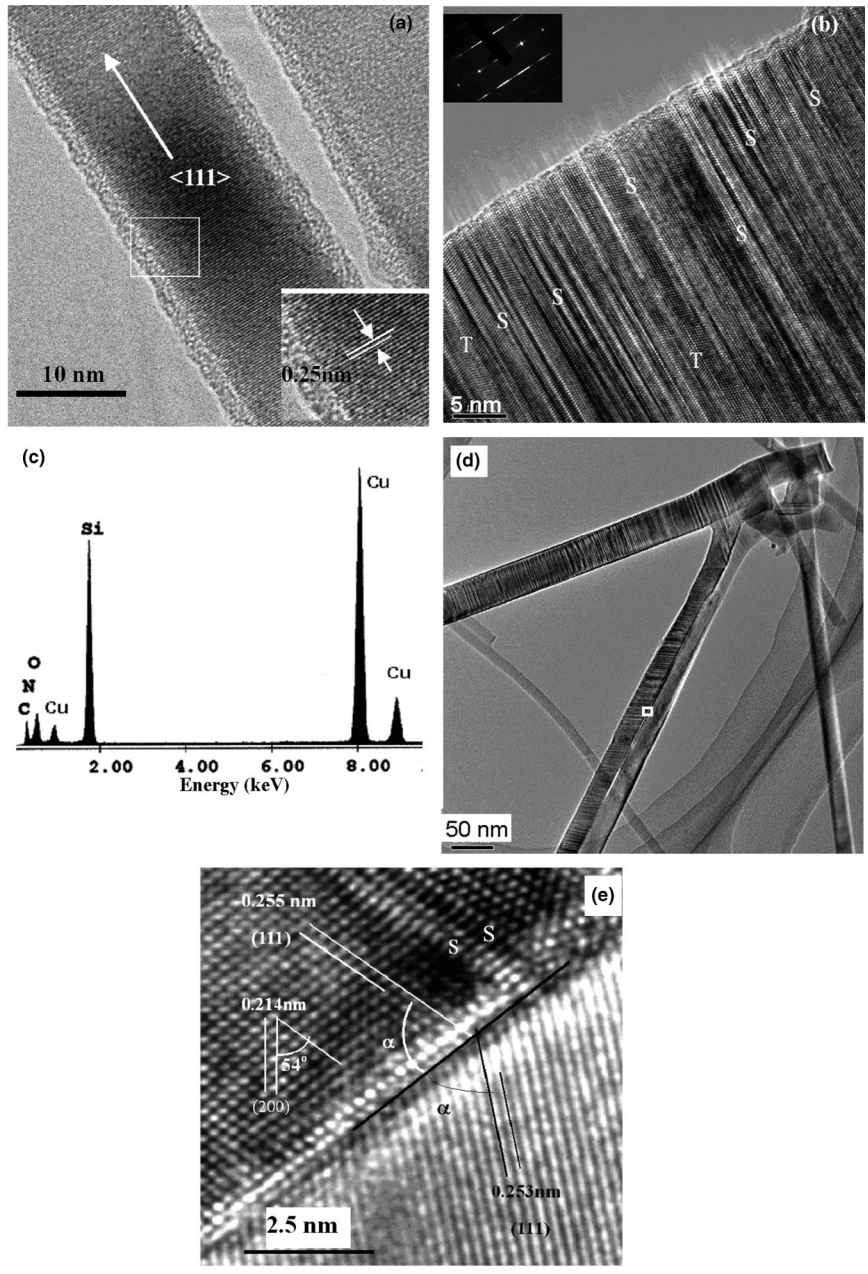

Figure 3. (a) HRTEM image of two SiCN nanowires with perfect lattice planes; the growth direction is indicated by a long arrow, and the inset is an HRTEM image at high magnification of the white square in (a), which clearly shows the spacing of about 0.25 nm corresponding to the distance between (111) planes of SiCN, (b) HRTEM image of a nanowire with high density of stacking faults indicated by "S" and microtwins indicated by "T" in it, and the inset is the SAED pattern taken on the nanowire also showing the stacking fault characteristic, (c) typical EDS spectrum recorded on the rod part of the nanowires, (d) TEM image showing a nanowire with "Y" junction and one of the branches with twin structure; the twin plane is in the middle of the branch, (e) HRTEM image of the zone indicated by a white square in (d) clearly shows half of the branch with stacking faults indicated by "S" and another half-with perfect lattice planes, and the twin angle (α) is about 60°.

accompany such twin structures, shown as in Figure 3d. This kind of semiconductive Y-junction nanowire may be of use in nanoelectronic devices.

It can be concluded from the above results that Products a and b are SiCN nanowires with Fe and FeS nanoparticles at their tips, respectively.

The existence of nanoparticles at the tips of the nanowires in Products a and b indicates that the growth mechanism of the nanowires is controlled by the vapor−liquid−solid (VLS) mechanism.[36] On the basis of the above results, a formation mechanism of the SiCN nanowires is proposed as follows. HMDSN vaporizes at above 126 °C, and ferrocene begins to vaporize at about 185 °C and decomposes at above 400 °C.[16] As the Si−C bond energy (75 kcal/mol) is lower than the Si−N bond energy (75.8 kcal/mol),[37] when the temperature is high enough, the cleavage of the Si−C bond occurs first to produce methyl (-CH_3) groups followed by the cleavage of the Si−N bond to produce ≡Si− and −NH− groups. The methyl groups decompose to form CH_4, C_2H_6, C, and H_2 (or two H· radicals) below 600 °C;[38] meanwhile, some of the H· radicals react with ≡Si− and −NH− groups to form SiH_4, Si_2H_6, and NH_3 gases. Carbon nanoparticles are carried by the gas stream, Ar gas mixed with the gases from pyrolysis of HMDSN, and deposit on the surface of firebrick and the small quartz tube to form a carbon film. The XRD samples could be contaminated by the carbon nanoparticles, and therefore the XRD pattern (see Figure 1b)

has a peak for carbon. When the thiophene is not used, the decomposed ferrocene is reduced by the H_2 to form atomic iron, which agglomerates into iron clusters. The clusters are carried by the gas mixture, Ar gas mixed with hydrocarbon gases, to the downstream site. At higher temperatures the clusters become iron droplets and deposit on the surface of firebrick. The C-, Si-, and N-contained gases are carried to the downstream area by the gas stream. The iron droplets serve as preferential sites for absorption of the gases. The gases are catalytically decomposed and Fe−Si−C−N alloy forms. As the Fe−Si−C−N alloy becomes supersaturated, SiCN segregates from the alloy droplets and grows along the <111> direction. Finally, SiCN nanowires with Fe nanoparticles at their tips form. When the thiophene is also used, thiophene decomposes and produces atomic sulfur at about 600 °C. The atomic sulfur reacts with the atomic iron to form FeS that agglomerates into FeS clusters. Just as only ferrocene is used as the catalyst precursor, the clusters are carried by the gas mixture to the downstream site. At high temperature the clusters become FeS droplets and deposit on the firebrick. The FeS droplets serve as preferential sites for absorption of the C-, Si-, and N-contained gases to form FeS−Si−C−N alloy. As the FeS−Si−C−N alloy becomes supersaturated, SiCN segregates from the alloy droplets and grows along the <111> direction. Finally SiCN nanowires with FeS nanoparticles at their tips form. It is known from the amount of the catalyst precursors used, the atomic ratio of S: Fe is above one, and extra S will react with FeS to form Fe_3S_4. Therefore, there is a peak corresponding to Fe_3S_4 in Figure 1b.

Because the melting point of FeS (~1190 °C) is much lower than that of Fe (1534 °C), the FeS−Si−C−N alloy solidifies at lower temperature than the Fe−Si−C−N alloy. This means that when both ferrocene and thiophene are used the nucleation and growth process of SiCN nanowires will last longer. Therefore, the yield of Product b is higher than that of Product a.

The droplets are very fine since they are formed in a very short time at high temperatures. Consequently, the products are very thin. The formation of SiO_2 outer layer must be due to a small amount of oxygen remaining in the quartz tube.

Because of the low content of nitrogen in the precursor (C:N = 6:1), the content of nitrogen in the SiCN nanowires is low. EDS analysis shows that the content of nitrogen is about 6−8 at. % when the contribution of carbon film from the TEM sample holder is neglected. If a polysilazane is used as a precursor, or the pyrolysis process is carried out in a flowing ammonia atmosphere, the nitrogen content could be increased.

Figure 4b shows I−V curve of a single-nanowire device shown as in Figure 4a, and the nanowire is from Product b. The good linearity of the I−V curve indicates good ohmic contact of the nanowire and electrodes. The resistivity of the nanowire is 1.0698×10^3 Ω·cm. Seong et al.[39] studied the electrical resistivity of SiC nanowires of <100 nm in diameter and several microns in length prepared by a CVD method. The resistivity of an individual SiC nanowire is 2.2×10^{-2} Ω·cm, which is much lower than our result. There could be several reasons for the difference. The SiCN crystal structure can be viewed as a SiC crystal structure in which some C atoms are replaced by N atoms. This replacement will increase the disorder of the crystal structure and increase the electrical resistivity, which could be the difference in resistivity. Another possible explanation is the effect of a thin insulating SiO_2 layer of our sample. A third possible reason may be related to crystal defects. Their SiC nanowires have a perfect single crystal nature with a <111> growth direction.[39] It is hard to know whether our SiCN nanowire measured has a perfect single crystal nature shown as in Figure 3a or numerous stacking faults shown as in Figure 3b or twin-structure shown as in Figure 3d. As stacking faults and twins will certainly affect the transport of electrons and increase the electrical resistivity, if the nanowire measured belongs to either of the latter two cases the resistivity will be high.

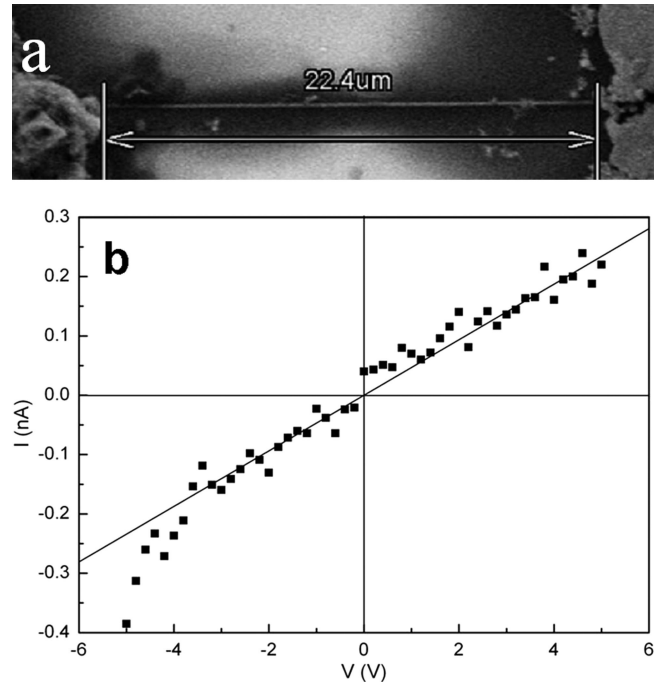

Figure 4. (a) SEM image of SiCN two-terminal nanowire device, (b) I−V characteristic of SiCN nanowire device contacted with silver electrodes on quartz plate.

Conclusions

Ultralong SiCN nanowires with FeS or Fe nanoparticles at their tips are synthesized via pyrolysis of HMDSN at 1100 °C catalyzed by ferrocene with or without thiophene, respectively. Adding ferrocene can decrease the synthesis temperature due to catalytic action of Fe from ferrocene, and adding both ferrocene and thiophene can promote the growth of SiCN nanowires due to the formation of FeS, which has a lower melting point than Fe. The growth of the nanowires is governed by the VLS mechanism. The as-synthesized nanowires are more uniform than those from pure HMSDN. The electrical resistivity of an individual SiCN nanowire is 1.0698×10^3 Ω cm at room temperature.

Acknowledgment. This work was supported by Natural Science Foundation of China (50371062, 50572052) and Shanghai Pujiang Program.

Supporting Information Available: A picture of white wool-like product grown on mullite firebrick. This information is available free of charge via the Internet at http://pubs.acs.org.

References

(1) Chen, L. C.; Chen, C. K.; Wei, S. L.; Bhusari, D. M.; Chen, K. H.; Chen, Y. F.; Jong, Y. C.; Hung, Y. S. *Appl. Phys. Lett.* **1998**, *729*, 2463.
(2) Saha, A.; Shah, S. R.; Raj, R.; Russek, S. E. *J. Mater. Res.* **2003**, *18*, 2549.
(3) Chen, L. C.; Chen, C. K.; Chen, K. H.; Chung, T. J.; Chen, L. C.; Lin, M. C. *J. Mater. Res.* **1997**, *12*, 322.

(4) Badzian, A.; Badzian, T.; Roy, R.; Drawl, W. *Thin Solid Films* **1999**, *354*, 148.
(5) Wong, E. W.; Sheehan, P. E.; Lieber, C. M. *Science* **1997**, *277*, 1971.
(6) Tarntair, F. G.; Wen, C. Y.; Chen, L. C.; Kuo, P. F.; Chang, S. W.; Chen, Y. F.; Hong, W. K.; Cheng, H. C. *Appl. Phys. Lett.* **2000**, *76*, 2630.
(7) Luo, Y.; Zheng, Z.; Xu, C.; Xie, Z.; Zhang, Z. *Mater. Sci. Eng., A* **2006**, *432*, 69.
(8) Cheng, W. J.; Jiang, J. C.; Zhang, Y.; Zhu, H. S.; Shen, D. Z. *Mater. Lett.* **2004**, *58*, 3467.
(9) Chang, H. L.; Lin, C. H.; Kuo, C. T. *Diamond Relat. Mater.* **2002**, *11*, 793.
(10) Jose-Yacaman, M.; Miki-Yoshida, M.; Rendon, L.; Santiesteban, J. G. *Appl. Phys. Lett.* **1993**, *62*, 657.
(11) Ivanov, V.; Fonseca, A.; Nagy, J. B.; Lucas, A.; Lambin, P.; Bernaerts, D.; Zhang, X. B. *Carbon* **1995**, *33*, 1727.
(12) Fonseca, A.; Hernadi, K.; Nagy, J. B.; Bernaerts, D.; Lucas, A. A. *J. Mol. Catal. A: Chem.* **1996**, *107*, 159.
(13) Endo, M.; Takeuchi, K.; Kobori, K.; Takahashi, K.; Kroto, H. W.; Sarkar, A. *Carbon* **1995**, *33*, 873.
(14) Sen, R.; Govindaraj, A.; Rao, C. N. R. *Chem. Phys. Lett.* **1997**, *267*, 276.
(15) Peigney, A.; Laurent, C.; Dobigeon, F.; Rousset, A. *J. Mater. Res.* **1997**, *12*, 613.
(16) Cheng, H. M.; Li, F.; Su, G.; Pan, H. Y.; He, L. L.; Sun, X.; Dresselhaus, M. S. *Appl. Phys. Lett.* **1998**, *72*, 3282.
(17) Kong, J.; Cassell, A. M.; Dai, H. J. *Chem. Phys. Lett.* **1998**, *292*, 567.
(18) Satishkumar, B. C.; Govindaraj, A.; Sen, R.; Rao, C. N. R. *Chem. Phys. Lett.* **1998**, *293*, 47.
(19) Campbell, P. M.; Snow, E. S.; Novak, J. P. *Appl. Phys. Lett.* **2002**, *81*, 4586.
(20) Ci, L. J.; Wei, J. Q.; Wei, B. Q.; Liang, J.; Xu, C. L.; Wu, D. H. *Carbon* **2001**, *39*, 329.
(21) Liu, B. C.; Lyu, S. C.; Jung, S. I.; Kang, H. K.; Yang, C. W.; Park, J. W.; Park, C. Y.; Lee, C. J. *Chem. Phys. Lett.* **2004**, *383*, 104.
(22) Zhu, H. W.; Xu, C. L.; Wu, D. H.; Wei, B. Q.; Vajtai, R.; Ajayan, P. M. *Science* **2002**, *296*, 884.
(23) Yang, W.; Miao, H.; Xie, Z.; Zhang, L.; An, L. *Chem. Phys. Lett.* **2004**, *383*, 441.
(24) Zhang, Y. J.; Wang, N. L.; He, R. R.; Chen, X. H.; Zhu, J. *Solid State Commun.* **2001**, *118*, 595.
(25) Dez, R.; Tenegal, F.; Reynaud Mayne, C.; M.; Armand, X.; Herlin-Boime, N. *J. Euro. Ceram. Soc.* **2002**, *22*, 2969.
(26) Yan, J.; Wang, A.; Kim, D. *Microporous Mesoporous Mater.* **2007**, *100*, 128.
(27) Tarntair, F. G.; Wu, J. J.; Chen, K. H.; Wen, C. Y.; Chen, L. C.; Cheng, H. C. *Surface Coating Technol.* **2001**, *137*, 152.
(28) Lin, H. Y.; Chen, Y. C.; Lin, C. Y.; Tong, Y. P.; Hwa, L. G.; Chen, K. H.; Chen, L. C. *Thin Solid Films* **2002**, *416*, 85.
(29) (a) Chiu, H. T.; Hsu, J. S. *Thin Solid Films* **1994**, *252*, 13. (b) Kleps, I.; Caccavale, F.; Brusatin, G.; Angelescu, A.; Armelao, L. *Vacuum* **1995**, *46*, 979. (c) Chen, Y.; Matsumoto, K.; Nishio, Y.; Shirafuji, T.; Nishino, S. *Mater. Sci. Eng., B* **1999**, *61*−*62*, 579. (d) Anma, H.; Toki, J.; Ikeda, T.; Hatanaka, Y. *Vacuum* **2000**, *59*, 665. (e) Seekamp, J.; Niemann, J.; Bauhofer, W. *J. Non-Cryst. Solids* **2000**, *704*, 266–269. (f) Xu, Y. Y.; Muramatsu, T.; Taniyama, M.; Aoki, T.; Hatanaka, Y. *Thin Solid Films* **2000**, *368*, 181. (g) Teker, K. *J. Cryst. Growth* **2003**, *257*, 245.
(30) Liang, Y.; Zheng, F.; Xian, Q.; Zhou, R. *Powder Technol.* **2003**, *137*, 29.
(31) Cai, K. F.; Lei, Q.; Zhang, A. X. *J. Nanosci. Nanotechnol.* **2007**, *7*, 580.
(32) Ci, L. J.; Rao, Z. L.; Zhou, Z. P.; Tang, D. S.; Yan, X. Q.; Liang, Y. X.; Liu, D. F.; Yuan, J.; Zhou, W. Y.; Wang, G.; Liu, W.; Xie, S. S. *Chem. Phys. Lett.* **2002**, *359*, 63.
(33) Zhou, Z. P.; Ci, L. J.; Chen, X. H.; Tang, D. S.; Yan, X. Q.; Liu, D. F.; Liang, Y. X.; Yuan, H. J.; Zhou, W. Y.; Wang, G.; Xie, S. S. *Carbon* **2003**, *41*, 337.
(34) Koumoto, K.; Takeda, S.; Pai, C.; Sata, T.; Yanagida, H. *J. Am. Ceram. Soc.* **1989**, *72*, 1985.
(35) Deepak, F. L.; Govindaraj, A.; Rao, C. N. R. *Chem. Phys. Lett.* **2001**, *345*, 5.
(36) Wagner, R. S.; Ellis, W. C. *Trans. Metal. Soc. AIME* **1965**, *233*, 1054.
(37) Beezer A. E.; Mortimer, C. T. *J. Chem. Soc. A* **1966**, *514*.
(38) Plawsky, J. L.; Wang, F.; Gill, W. N. *AIChE J.* **2002**, *48*, 2315.
(39) Seong, H. K.; Choi, H. J.; Lee, S. K.; Lee, J. I.; Choi, D. J. *Appl. Phys. Lett.* **2004**, *85*, 1256.

CG701079X